Research Square

Preprints are preliminary reports that have not undergone peer review.
They should not be considered conclusive, used to inform clinical practice,
or referenced by the media as validated information.

Adaptive Robust Filtering Based on SE(3) and Its Application in SINS/DVL Navigation

Liu MingMing
Guangdong Polytechnic of Communications
Liu Jinlai
15871371582@163.com

China Shipbuilding Industry Corporation Emergency Warning and Rescue Equipment Co., Ltd

Article

Keywords: Integrated Navigation, Lie Group/Lie Algebra, Huber Method, Transformed Cubature Kalman Filter

Posted Date: November 16th, 2026

DOI: https://doi.org/10.21203/rs.3.rs-11442439/v1

License: This work is licensed under a Creative Commons Attribution 4.0 International License.
Read Full License

Additional Declarations: No competing interests reported.

Adaptive Robust Filtering Based on SE(3) and Its Application in SINS/DVL Navigation

Liu MingMing [a] Liu Jinlai[b,*]

a Guangdong Polytechnic of Communications, Guangzhou 510650, China;

b China Shipbuilding Industry Corporation Emergency Warning and Rescue Equipment Co., Ltd, Wuhan, 430223, China;\

*Correspondence: 15871371582@163.com

Abstract: Aiming at the problems of state-space inconsistency and vulnerability to measurement outliers caused by the traditional Euler-angle error model in the SINS/DVL integrated navigation system under complex environments, this paper proposes a robust adaptive algorithm based on the special Euclidean group SE(3). Firstly, by introducing the Lie group/Lie algebra theory, the estimated states of the transformed cubature Kalman filter (TCKF) are embedded into the SE(3) space, and left/right error TCKF (LSE/RSE-TCKF) is constructed, which essentially improves the spatial consistency of attitude and velocity state estimation. Furthermore, an adaptive mechanism is designed by combining the chi-square test with the Huber method to detect innovation vectors in real time and reconstruct abnormal measurements during the measurement update phase, thus forming the SE(3) robust adaptive transformed cubature Kalman filter (SE(3)-RATCKF). Ship-borne SINS/DVL experimental results show that, compared with traditional methods, the proposed algorithm not only effectively solves the state-space inconsistency problem and significantly improves navigation accuracy under large misalignment angles, but also exhibits superior robustness. It can adaptively suppress measurement outlier interference in complex environments and avoid excessive compensation under normal measurement conditions, which verifies its effectiveness in improving the estimation accuracy and stability of integrated navigation systems.

Key words: Integrated Navigation; Lie Group/Lie Algebra; Huber Method; Transformed Cubature Kalman Filter

0 Introduction

Integrated navigation systems based on the Strapdown Inertial Navigation System (SINS), supplemented by the Global Position System (GPS), Doppler Velocity Log (DVL), Ultra Short Base Line (USBL), etc., have been widely applied in civil and military fields [1-3]. Among them, SINS/DVL is commonly used for surface navigation or underwater target tracking, and serves as one of the mainstream integrated navigation systems in maritime applications [4-5]. For systems such as SINS/DVL, modern filtering techniques are critical factors affecting navigation performance. The Kalman Filter (KF) has attracted extensive attention owing to its ability to derive recursive minimum-variance estimation under Gaussian distribution conditions [6-7], yet it fails to handle nonlinear constraints effectively. Accordingly, numerous nonlinear filtering methods based on KF

*Correspondence: 15871371582@163.com

theory have been successively proposed, including the Extended Kalman Filter (EKF) [8], Unscented \Kalman Filter (UKF) [9], Cubature Kalman Filter (CKF) [10], and Orthogonal Transformed Cubature Kalman Filter (TCKF) [11]. Specifically, TCKF performs orthogonal transformation on the sampling points of CKF, which mitigates the non-local sampling problem to a certain extent [12].

State errors in the above traditional filtering methods are defined as the difference between ideal and actual values. Taking velocity error as an example, it is directly obtained by subtracting the calculated actual velocity from the ideal velocity. Affected by various error sources, the actual values in navigation systems lie in the computational coordinate system with error terms, while ideal values are in the ideal coordinate system [13]. Nevertheless, vectors can only be directly added or subtracted when they belong to the same coordinate system. Therefore, the conventional definition of displacement errors such as velocity and position ignores vector direction and only considers magnitude, which easily leads to state-space inconsistency. Fundamentally, this definition of displacement errors arises from the fact that attitude errors in the traditional Euler-angle error model belong to the Special Orthogonal Group (SO(3)), whereas errors in velocity and position are defined in Euclidean space. The inconsistency of spaces for velocity, position and attitude states prevents attitude (direction) information from being coupled in displacement error definition.

In fact, by establishing coupling relationships between rotational and translational motions of rigid bodies, attitude and displacement states of navigation systems can be approximately defined in a unified space, which improves the spatial inconsistency of error definitions and further enhances estimation performance [14]. With the development of group theory, Lie group/Lie algebra theory extends the solvability of algebraic equations to differential equations [15]. By introducing state variables such as attitude and velocity into the Special Euclidean Group (SE(3)), attitude information is coupled into displacement errors, providing a new perspective for research on state-space consistency of integrated navigation while improving state estimation accuracy [16]. Reference [17] derived a Lie group error model in the Earth-centered coordinate system, verifying its filtering consistency and superiority under large misalignment angles. Reference [18] analyzed left and right SE(3) Euler-angle error models of SINS/GPS and SINS/DVL in the navigation coordinate system, pointing out the research necessity of Lie group error models. References [19-20] reconstructed state error equations of EKF based on Lie group affine theory and proposed the Invariant EKF (IEKF), which maintains spatial consistency for EKF state estimation. Reference [21] presented a Lie-group left-error EKF (Ln-EKF) for Miniature Inertial Measurement Unit/Global Navigation Satellite System (MIMU/GNSS) in the Earth-centered coordinate system, demonstrating that Ln-EKF achieves higher accuracy than traditional filtering methods. Based on Lie group theory, Reference [22] proposed $SE_2(3)$ left-error and right-error UKFs (LSE-UKF and RSE-UKF) for SINS/GNSS, avoiding the calculation of state transition matrices in IEKF and improving state estimation performance. Both $SE_2(3)$ and SE(3) are built on Lie group and Lie algebra theory, with the difference that $SE_2(3)$ incorporates position errors as an additional state, while SE(3) only unifies attitude and velocity in a single coordinate frame. Parameters capable of rotation and translation

must be vectors, and velocity parameters satisfy the vector form in local coordinate systems. However, some studies indicate that position cannot be easily expressed as a “vector diameter”, and position error terms coupled with attitude errors may cause negative compensation under large misalignment angles [23].

Meanwhile, the estimation accuracy of modern filtering techniques relies on external measurements provided by sensors. Complex conditions such as high maneuverability and electromagnetic interference tend to introduce measurement outliers, degrading estimation performance. Aiming at outlier suppression in filtering, scholars have conducted extensive research on robust strategies. Reference [24] introduced the maximum entropy criterion into the interacting multiple-model KF to improve filtering performance in complex environments. Reference [25] modified the quadratic index via generalized cost functions during the measurement update of UKF, and proposed a robust UKF based on the Huber estimation method to enhance the robustness of integrated navigation systems under non-Gaussian noise. References [26-27] adopted Huber-M estimation to improve the filtering accuracy of CKF in navigation applications.

To address the above issues, this paper proposes a robust adaptive TCKF based on SE(3) for SINS/DVL integrated navigation. The main contributions are summarized as follows:

(1) SE(3)-based TCKF for spatial consistency: By introducing Lie group/Lie algebra theory, the estimated states of the TCKF are embedded into the SE(3) space, and the left/right error TCKFs (LSE-TCKF and RSE-TCKF) are constructed. This reformulation unifies attitude and velocity errors in a single coordinate frame and improves the state-space consistency of the conventional SO(3)-TCKF.

(2) Adaptive robust strategy against outliers: By combining the chi-square test with the Huber method, an adaptive mechanism is designed to detect innovation vectors in real time during the measurement update phase. The Huber estimation is activated only when the test statistic exceeds the chi-square threshold, which reconstructs abnormal measurements without over-compensating normal ones.

(3) SE(3)-RATCKF and experimental validation: The above two strategies are integrated to form the SE(3)-RATCKF. Ship-borne SINS/DVL experiments under different initial misalignment angles and outlier conditions verify that the proposed method effectively resolves the state-space inconsistency, significantly improves navigation accuracy, and exhibits superior robustness compared with traditional methods.

It should be noted that while the chi-square threshold setting in this paper is inspired by our prior work [28] on multi-path delayed calculation for standalone SINS, the present study is fundamentally different in both theoretical formulation and application scope. Specifically, unlike the conventional Euclidean error model used in [28] to suppress Schuler oscillations without external measurements, this paper fundamentally resolves the state-space inconsistency under large misalignment angles by embedding attitude and velocity into the Lie group SE(3). Furthermore, the robust mechanism in this paper is entirely reformulated within the Lie algebra tangent space,

explicitly deriving the Huber nonlinear regression equations for the SE(3) left and right error states to ensure mathematical consistency, and is specifically tailored to address the combined challenges of large misalignments and DVL outliers in SINS/DVL integrated navigation.

1 Navigation Problem Description and Notation

For the SINS/DVL integrated navigation system, the commonly used coordinate systems are defined as follows: the geographic coordinate system with an east–north–up orientation is defined as the navigation frame (*n*-frame); the body frame (*b*-frame) with a right–forward–up orientation is defined as the body coordinate system; quantities with tilde denote navigation parameters with computational errors, and these definitions are used consistently in the subsequent TCKF formulation.

The state estimated by the TCKF is composed of the attitude error, velocity error, position error, and the accelerometer and gyroscope measurement errors. For convenience of derivation, the sampling points of each state are expressed as dφ, dv, dp, d∇, and dε in Eq. (4). The transition of these state components is described by the SINS/DVL Euler-angle error update equations, i.e., Eqs. (5)–(8), where the involved navigation parameters and their computational-error versions follow the definitions given in Section 2.

The external measurement considered in this paper is the DVL velocity measurement. The measurement used by the TCKF is the velocity difference between the SINS and DVL; its left- and right-error forms are expressed in Eqs. (31) and (41), respectively, while the measurement matrix H used in the SO(3)-TCKF is defined below Eq. (12). On this basis, the TCKF recursively performs sampling-point calculation, one-step state prediction, measurement prediction, state estimation, and feedback correction, as summarized by Eqs. (3)–(14). The feedback correction compensates the attitude, velocity, and position according to Eq. (14). Hence, the estimation problem addressed in this paper is to recursively estimate the above state from the SINS/DVL state transition and the DVL velocity measurement and to correct the SINS outputs, while the spatial consistency of the error definition and the influence of measurement outliers are handled by the SE(3) left/right error formulation and the robust adaptive strategy given in Sections 3.2–3.4.

The motivation for the subsequent reformulation is as follows. In the conventional definition, the velocity error is obtained by directly subtracting the computed velocity from the ideal velocity, while the ideal and computed velocities are associated with the ideal and computational coordinate systems, respectively. Such direct subtraction ignores the directional difference between the two coordinate systems and thus leads to the state-space inconsistency. To avoid this, the SE(3) left and right errors τ_L and τ_R are defined in Eqs. (23) and (35), respectively, and the corresponding TCKF prediction, measurement prediction, and feedback correction are given in Sections 3.2 and 3.3. Measurement outliers are treated by the chi-square test and Huber method in Section 3.4. These definitions and formula references are used consistently in the remainder of the paper.

2 SO(3)-Based TCKF

As a background and baseline filter, this section briefly reviews the standard SO(3)-TCKF based on the coordinate frames and notation defined in Section 1; this filter will be reformulated in Section 3. The aim of the TCKF here is to approximate the Bayesian prediction and measurement update of the SINS/DVL error state by a set of deterministic sampling points, so that the nonlinear state transition and measurement functions can be handled without linearization; the orthogonal transformation of the cubature points is used to improve the numerical integration accuracy of this approximation. In the SO(3)-TCKF, the estimated state is the conventional Euler-angle error state, and the estimated attitude, velocity and position errors are fed back to the SINS mechanization according to Eq. (14).

The validity of this baseline relies on two conditions. First, the conventional Euler-angle error model is used under the small-misalignment-angle assumption, under which the ideal navigation frame and the computational navigation frame are close enough and the direct subtraction of velocity and position vectors is acceptable. Second, the DVL measurement noise is assumed to be approximately Gaussian and free of abnormal outliers. These conditions are reasonable for ordinary navigation cases, but they may be violated in complex aquatic environments with large misalignment angles or measurement outliers. Such violations are exactly the motivations for the SE(3)-TCKF and the robust adaptive strategy developed in Sections 3.2–3.4.

(1) Parameter Initialization

Initialize the state vector and its covariance matrix used by the TCKF, together with the state noise covariance matrix Q_k and the measurement noise covariance matrix R_k appearing in Eqs. (3)–(14). The initial values are set according to the prior information of the SINS/DVL system. The remaining TCKF quantities, such as the sampling points and weights, are generated in the following steps according to the standard TCKF procedure [11-12].

(2) Sampling Point Calculation

The aim of this step is to generate a set of sampling points that satisfy the third-order numerical integration rule, so that the nonlinear state transition and measurement functions can be approximated in the subsequent prediction and update steps. TCKF performs an orthogonal transformation on the Sigma points of CKF to obtain the new sampling points; the detailed construction is standard and can be found in [11-12]. On the basis of CKF, TCKF performs orthogonal transformation on sigma points to generate a new set of sampling points that satisfy third‑order precision numerical integration. As a fundamental procedure of TCKF, this step involves standard formulas which have been elaborated in relevant TCKF studies. Thus, the detailed calculation is not repeated in this paper.

(3) State Prediction

Using the sampling points obtained above, this step propagates each point through the SINS/DVL state transition equation to obtain the one-step predicted state mean and covariance, as given by Eqs. (3)–(9). After obtaining the sampling points of TCKF, the predicted sampling points in the state prediction process can be calculated as

$$P_{k-1}^{+} = S_{k-1}^{+}(S_{k-1}^{+})^{\mathrm{T}} \tag{1}$$

$$\chi_j^{+} = S_{k+1}^{+}\lambda_j + x_{k-1} \tag{2}$$

where P_{k-1}^{+} denotes the state covariance matrix at time k-1 , S_{k-1}^{+} is the matrix obtained by Cholesky decomposition of P_{k-1}^{+} , λ_j represents the sampling points of TCKF with j =1,2,…,2n , and n is the state dimension. x_{k-1} is the state vector of SINS/DVL at time k-1. $x_k = [\delta\varphi_E \ \delta\varphi_N \ \delta\varphi_U \ \delta v_E \ \delta v_N \ \delta v_U \ \delta L \ \delta\lambda \ \delta h \ \nabla_x \ \nabla_y \ \nabla_z \ \varepsilon_x \ \varepsilon_y \ \varepsilon_z]^{\mathrm{T}}$, Herein, $\delta\varphi_E$, $\delta\varphi_N$, $\delta\varphi_U$ are the Euler-angle errors; δv_E , δv_N , δv_U denote the three-axis velocity errors in the east-north-up (ENU) frame; δL , $\delta\lambda$, δh represent the errors of longitude, latitude and altitude; ∇_x , ∇_y , ∇_z and ε_x , ε_y , ε_z are the three-axis measurement errors of gyros and accelerometers, respectively.

Equations (1)–(3) are the standard cubature-point generation and one-step prediction formulas of the CKF/TCKF; their derivations are not repeated here, and the reader is referred to [10–12] for details. The one‑step state prediction can be calculated according to Equation (2)

$$\overline{x}_k = \sum_{j=1}^{2n} \omega_j f(\chi_j^{+}) \tag{3}$$

where $f(\cdot)$ denotes the state transition function, specifically the state update equation of the SINS/DVL system, and ω_j represents the weight of TCKF with $\omega_j = 1/(2n)$. For the convenience of derivation, let the form of χ_j^{+} in the j_{th} calculation be defined $[d\varphi \ dv \ dp \ d\nabla \ d\varepsilon]^{\mathrm{T}}$, where the sampling points of each state can be expressed as

$$\begin{cases} \mathrm{d}\varphi = \left[\mathrm{d}\varphi_E \quad \mathrm{d}\varphi_N \quad \mathrm{d}\varphi_U\right]^{\mathrm{T}} \\ \mathrm{d}v = \left[\mathrm{d}v_E \quad \mathrm{d}v_N \quad \mathrm{d}v_U\right]^{\mathrm{T}} \\ \mathrm{d}p = \left[\mathrm{d}L \quad \mathrm{d}\lambda \quad \mathrm{d}h\right]^{\mathrm{T}} \\ \mathrm{d}\nabla = \left[\mathrm{d}\nabla_x \quad \mathrm{d}\nabla_y \quad \mathrm{d}\nabla_z\right]^{\mathrm{T}} \\ \mathrm{d}\varepsilon = \left[\mathrm{d}\varepsilon_x \quad \mathrm{d}\varepsilon_y \quad \mathrm{d}\varepsilon_z\right]^{\mathrm{T}} \end{cases} \tag{4}$$

where d denotes the time derivative of each variable.

Error model in [13] is derived from the SINS/DVL Euler-angle error update equations, shown as

$$f(\chi_j^{+}) = \begin{bmatrix} f(\mathrm{d}\varphi) \\ f(\mathrm{d}v) \\ f(\mathrm{d}p) \\ \mathrm{d}\nabla \\ \mathrm{d}\varepsilon \end{bmatrix} = \begin{bmatrix} \mathrm{d}\varphi + \left[-(\tilde{\omega}_{in}^{n})_{\times}\mathrm{d}\varphi + (\delta\tilde{\omega}_{ie}^{n} + \delta\tilde{\omega}_{en}^{n}) - \tilde{C}_b^{n}\mathrm{d}\nabla\right]T \\ \mathrm{d}v + \begin{bmatrix} (\tilde{C}_b^{n}\mathrm{d}\varepsilon)_{\times} f(\mathrm{d}\varphi) - (2\tilde{\omega}_{ie}^{n} + \tilde{\omega}_{en}^{n})_{\times}\mathrm{d}v + \\ (\tilde{v}^{n})_{\times}(2\delta\tilde{\omega}_{ie}^{n} + \delta\tilde{\omega}_{en}^{n}) + \tilde{C}_b^{n}\mathrm{d}\varepsilon \end{bmatrix} T \\ \mathrm{d}p + (M_1 f(\mathrm{d}v) + M_2\delta p)T \\ \mathrm{d}\nabla \\ \mathrm{d}\varepsilon \end{bmatrix} \tag{5}$$

where $(\cdot)_{\times}$ denotes the skew-symmetric matrix of the corresponding variable, "~" represents navigation parameters with computational errors, $\omega_{in}^{n} = \omega_{ie}^{n} + \omega_{en}^{n}$ is the carrier angular velocity

in the *n*-frame, ω_{ie}^{n} denotes the Earth-rotation angular velocity in the *n*-frame, ω_{en}^{n} is the transport angular velocity, C_{b}^{n} is the direction cosine matrix from the *b*-frame to the *n*-frame, $v^{n}=[v_E\ v_N\ v_U]^{\mathrm{T}}$ stands for the carrier velocity in the *n*-frame, and *T* is the sampling period. The deviations of ω_{ie}^{n} and ω_{en}^{n} are given as

$$\begin{cases} \delta\omega_{ie}^{n}=\begin{bmatrix} 0 \\ -\omega_{ie}\sin L\mathrm{d}L \\ \omega_{ie}\cos L\mathrm{d}L \end{bmatrix} \\ \delta\omega_{en}^{n}=\begin{bmatrix} \text{-}\mathrm{d}v_N/(R_M+h) \\ M_m\cos L\text{ - }N_n\sin L\mathrm{d}L \\ M_m\sin L+N_n\cos L\mathrm{d}L \end{bmatrix} \end{cases} \tag{6}$$

$$M_m=\frac{\mathrm{d}v_E+\tilde{v}_E\tan L\mathrm{d}L}{(R_N+h)\cos L},N_n=\frac{\tilde{v}_E}{(R_N+h)\cos L} \tag{7}$$

$$\begin{cases} M_1=\begin{bmatrix} 0 & \dfrac{1}{R_M+h} & 0 \\ \dfrac{1}{(R_N+h)\cos L} & 0 & 0 \\ 0 & 0 & 1 \end{bmatrix} \\ M_2=\begin{bmatrix} 0 & 0 & 0 \\ \dfrac{\tilde{v}_N\tan L}{(R_N+h)\cos L} & 0 & 0 \\ 0 & 0 & 0 \end{bmatrix} \end{cases} \tag{8}$$

where ω_{ie} is the Earth-rotation angular velocity, and R_N and R_M denote the radii of curvature of the prime vertical and meridian of the Earth, respectively.

Based on Equation (3), the covariance matrix of one-step state prediction is obtained.

$$P_k^{-}=\sum_{j=1}^{2n}\omega_j(f(\chi_j^{+})-\bar{x}_k)(f(\chi_j^{+})-\bar{x}_k)^{\mathrm{T}}+Q_k \tag{9}$$

where Q_k denotes the state noise covariance matrix.

(4) Measurement Update

This step propagates the predicted sampling points through the measurement equation to obtain the predicted measurement, the innovation covariance and the cross-covariance, as given by Eqs. (10) – (13). The measurement matrix *H* is defined below Eq. (12). Firstly, the estimated sampling points in the measurement update process are calculated as

$$P_k^{-}=S_k^{-}(S_k^{-})^{\mathrm{T}} \tag{10}$$

$$\chi_j^{-}=S_k^{-}\lambda_j+\bar{x}_k \tag{11}$$

where S_k^{-} is the matrix obtained by Cholesky decomposition of P_k^{-}.

The predicted measurement can be derived from Equation (11) as

$$\bar{z}_k=\sum_{j=1}^{2n}(H\chi_j^{-})\omega_j \tag{12}$$

where $H=-[(\tilde{v}_{DVL}^{n})_{\times}\ \mathrm{I}_{3\times3}\ 0_{3\times3}]$ denotes the measurement matrix, and $\tilde{v}_{DVL}^{n}$ is obtained by

rotating the actual velocity $\tilde{v}_{DVL}^{b}$ output of DVL. Furthermore, the corresponding predicted measurement covariance matrix can be derived as

$$P_k^{zz} = \sum_{j=1}^{2n} (H\chi_j^- - \overline{z}_k)(H\chi_j^- - \overline{z}_k)^{\mathrm{T}} \omega_j + R_k \tag{13}$$

where R_k denotes the measurement noise covariance matrix.

(5) State Estimation

Based on the quantities obtained in the measurement update, the Kalman gain, the state estimate and the covariance matrix are updated. The aim of this step is to fuse the DVL velocity measurement with the one-step prediction so that the posterior error-state estimate and its covariance are obtained. These are standard TCKF equations and are therefore not repeated here; the complete formulas are available in [11-12]. The state estimation of SO(3)-TCKF involves the calculation of cross-covariance matrix, Kalman filter gain, state estimation update and covariance matrix update. The formulas for the above steps are consistent with those of CKF and TCKF, which are standard equations for nonlinear Kalman filtering. Detailed derivations can be found in References [11-12] and are not repeated here.

(6) Feedback Correction

The aim of this step is to feed the estimated attitude, velocity and position errors back to the SINS mechanization according to Eq. (14), so that the navigation solution is corrected before the next filtering cycle. The feedback correction of SO(3)-TCKF follows the standard feedback form used in CKF/TCKF [11–12] and compensates the errors of attitude, velocity and position as

$$\begin{cases} C_b^n = \exp(\delta\varphi)\tilde{C}_b^n \\ v^n = \tilde{v}^{\mathrm{n}} - \delta v \\ p = \tilde{p} - \delta p \end{cases} \tag{14}$$

where $\delta\varphi = [\delta\varphi_E \ \ \delta\varphi_N \ \ \delta\varphi_U]^{\mathrm{T}}$, $\delta v = [\delta v_E \ \ \delta v_N \ \ \delta v_U]^{\mathrm{T}}$, $\delta p = [\delta L \ \ \delta\lambda \ \ \delta h]^{\mathrm{T}}$.

It can be seen from Equation (14) that the velocity error is defined as $\delta v = \tilde{v}^n - v^n$. In fact, v^n belongs to the *n*-frame while $\tilde{v}^{\mathrm{n}}$ belongs to the *n′*-frame, making direct subtraction imprecise. Therefore, the directional difference between the two frames should also be taken into account. This problem is difficult to address due to the inconsistent spaces where attitude and displacement states are defined in SO(3)-TCKF.

3 SE(3)-Based TCKF

To improve the spatial consistency of SO(3)-TCKF, the error states are redefined based on Lie group/Lie algebra theory, and the state prediction, measurement prediction and feedback correction are reformulated. By embedding the states of the SINS/DVL integrated navigation system into the SE(3) space, the SE(3)-based TCKF is proposed.

3.1 Theoretical Basis

This section discusses the theoretical basis of SE(3)-TCKF, mainly including Lie group/Lie algebra theory and the SE(3) representation of SINS/DVL states. A Lie group is a smooth manifold endowed with a group structure, and its Lie algebra is the tangent space at the identity element, equipped with the Lie bracket operation. The Lie algebra captures the local structure of the Lie group through the exponential map. SO(3) and SE(3) are Lie groups describing rigid-body rotation and rigid-body motion, respectively, and so(3) and se(3) are their corresponding Lie algebras. The elements of so(3) are three-dimensional rotation vectors, while the elements of se(3) are six-dimensional vectors composed of a rotation part and a translation-related part; the Lie bracket of

se(3) is defined by the commutator of the corresponding 4×4 matrices. Standard treatments of these concepts can be found in [15] and [19]. SO(3) can only describe the rotational motion of a rigid body, whereas SE(3) includes both translation and rotation as follows:

$$\mathrm{SO}(3)=r\in\mathrm{SO}(3)|\ rr^{\mathrm{T}}=\mathrm{I}_{3\times3},\quad |r|=1 \tag{15}$$

$$\mathrm{SE}(3)=\left\{E=\begin{bmatrix} r & t \\ 0 & 1 \end{bmatrix}\right\}\in\mathrm{R}^{4\times4}|\ r\in\mathrm{R}^{3\times3},t\in\mathrm{R}^{3} \tag{16}$$

where r and t denote the rotation matrix and translation vector respectively, $\mathrm{R}^{4\times4}$ represents a 4×4 matrix, and I is the identity matrix.

It can be seen from Equations (15) and (16) that SE(3) can describe rigid-body motion more accurately than SO(3), and its corresponding Lie algebra is given as follows:

$$\mathrm{se}(3)=\left\{\zeta=\begin{bmatrix}\phi\\ \xi\end{bmatrix}\in\mathrm{R}^{6},\ \phi\in\mathrm{so}(3),\xi\in\mathrm{R}^{3},(\xi)_{\times}=\begin{bmatrix}(\phi)_{\times} & \xi\\ 0 & 1\end{bmatrix}\right\} \tag{17}$$

where ϕ denotes the rotation vector and the remaining part of the vector in Eq. (17) denotes the translation-related component. Although ϕ still represents attitude angle errors, it is no longer the difference of Euler angles under the Euler-angle framework but a rotation vector. The vector in Eq. (17) is an element of se(3), i.e., a vector of the Lie algebra associated with SE(3). The operation considered for this algebra is the Lie bracket, which for se(3) is the commutator of the corresponding 4×4 matrices; its explicit form and derivation are standard and are not repeated here, with details available in [15] and [19]. Correspondingly, so(3) is the Lie algebra associated with SO(3).

The transformation relationship between SE(3) and se(3) is given by the exponential map in Eq. (18), which maps an element of the Lie algebra to the corresponding Lie group element; the standard definition and properties of this exponential map can be found in [15] and [19].

$$\exp((\zeta)_{\times})=\begin{bmatrix}\exp((\phi)_{\times}) & Jv\\ 0_{1\times3} & 1\end{bmatrix} \tag{18}$$

where Jv denotes the velocity error. Since the SE(3)-TCKF is an error-state filter, the error vector ϕ is defined in the local tangent space (Lie algebra) and is reset to near zero at each measurement update through the feedback correction. Therefore, at each filtering step, the local error ϕ is sufficiently small to satisfy the first-order local approximation of the exponential mapping... and the Jacobian matrix J can be locally approximated as the identity matrix. It should be noted that this is a standard local linearization in Lie group filtering, and the initial large misalignment angles (e.g., 30°) are absorbed by the initial state covariance matrix, not by this local approximation. Based on Lie group and Lie algebra theory, the attitude transformation matrix C_b^n and velocity v^n are incorporated into the special Euclidean group SE(3), which is expressed as:

$$\chi=\begin{bmatrix}C_b^n & v^n\\ 0_{1\times3} & 1\end{bmatrix}\in\mathrm{SE}\ (3) \tag{19}$$

The following proves that the states of the SINS/DVL integrated navigation system satisfy the group-affine property. Taking the inverse of Equation (19) yields the following:

$$\chi^{-1}=\begin{bmatrix}C_n^b & -C_n^b v^n\\ 0_{1\times3} & 1\end{bmatrix}\in\mathrm{SE}\ (3) \tag{20}$$

Then the differential equation of χ can be written as:

$$
\begin{aligned}
\dot{\chi} &= f(\chi) \\
&= \begin{bmatrix} C_b^n(\omega_{ib}^b)_\times - (\omega_{in}^n)_\times C_b^n & C_b^n f_{ib}^b - (2\omega_{ie}^n + \omega_{en}^n)_\times v^n + g^n \\ 0_{1\times 3} & 1 \end{bmatrix} \\
&= \begin{bmatrix} C_b^n & v^n \\ 0_{1\times 3} & 1 \end{bmatrix} \begin{bmatrix} (\omega_{ib}^b)_\times & f_{ib}^b \\ 0_{1\times 3} & 0 \end{bmatrix} + \begin{bmatrix} (\omega_{in}^n)_\times & g^n - (\omega_{ie}^n)_\times v^n \\ 0_{1\times 3} & 0 \end{bmatrix} \begin{bmatrix} C_b^n & v^n \\ 0_{1\times 3} & 1 \end{bmatrix} \\
&= \chi W_1 + W_2 \chi
\end{aligned}
\tag{21}
$$

where f_{ib}^b denotes the specific force and ω_{ib}^b is the gyroscope output. Setting $\chi_1 = \chi_2 = \chi$ yields:

$$
\begin{aligned}
f(\chi_1\chi_2) &= \chi_1\chi_2 W_1 + W_2\chi_1\chi_2 \\
&= f(\chi_1)\chi_2 + \chi_1 f(\chi_2) - \chi_1 f(\mathrm{I}_{5\times 3})\chi_2
\end{aligned}
\tag{22}
$$

It can be seen from Equation (22) that the SINS/DVL navigation states satisfy the group-affine property, namely the invariance property, which enables their redefinition.

3.2 Left-Error SE(3)-TCKF

Depending on the definition of error, error states are categorized into left-error and right-error states, which are defined as $\tau_L = \tilde{\chi}^{-1}\chi$ and $\tau_R = \chi\tilde{\chi}^{-1}$ respectively. This section derives the left-error SE(3)-TCKF (LSE-TCKF).

Let the estimated state of the SINS/DVL system by the LSE-TCKF be $x_L = [\delta\varphi_L \ \ \delta v_L \ \ \delta p_L \ \ \delta\nabla \ \ \delta\varepsilon]^{\mathrm{T}}$. Based on the conclusions in Section 2.1, the redefined left-error state satisfying group invariance properties is derived as follows:

$$
\begin{aligned}
\tau_L &= \tilde{\chi}^{-1}\chi \\
&= \begin{bmatrix} \tilde{C}_n^b C_b^n & \tilde{C}_n^b(v^n - \tilde{v}^n) \\ 0_{1\times 3} & 1 \end{bmatrix} \\
&= \begin{bmatrix} \tau_L^a & \tau_L^v \\ 0_{1\times 3} & 1 \end{bmatrix} \in \mathrm{SE(3)}
\end{aligned}
\tag{23}
$$

where τ_L^a and τ_L^v denote the newly defined left-invariant attitude error and velocity error, respectively, with $\tau_L^a = \exp((\varphi_L)_\times) = \tilde{C}_n^b C_b^n = C_b^{b'}$ and $\tau_L^v = \tilde{C}_n^b(v^n - \tilde{v}^n) = -\tilde{C}_n^b \delta v^n$. Due to different error definitions, the differences between LSE-TCKF and SO(3)-TCKF lie in the state prediction, measurement prediction and feedback correction related to state errors. First, the state prediction of LSE-TCKF is derived. Combined with Equation (23), differentiating τ_L^a and τ_L^v yields the differential equations of attitude and velocity as follows:

$$
\begin{aligned}
\frac{\mathrm{d}\tau_L^a}{\mathrm{d}t} &= \frac{\mathrm{d}\tilde{C}_n^b C_b^n}{\mathrm{d}t} \\
&= \frac{\mathrm{d}C_{b'}^b}{\mathrm{d}t} \\
&\approx \frac{\mathrm{d}((\delta\varphi_L)_\times)}{\mathrm{d}t} \\
&= -[(\tilde{\omega}_{ib}^b)_\times \delta\varphi_L]_\times - (\delta\omega_{ib}^b)_\times + (C_n^{b'}\delta\omega_{in}^n)_\times
\end{aligned}
\tag{24}
$$

$$
\frac{\mathrm{d}\delta\varphi_L}{\mathrm{d}t} = -(\tilde{\omega}_{ib}^b)_\times \delta\varphi_L - \delta\omega_{ib}^b + C_n^{b'}\delta\omega_{in}^n \tag{25}
$$

$$\begin{aligned}\frac{\mathrm{d}\tau_L^v}{\mathrm{d}t} &= \frac{\mathrm{d}C_n^{b'}(v^n-\tilde{v}^n)}{\mathrm{d}t}\\ &= -\left[(C_n^{b'})^{\mathrm{T}}\tilde{\omega}_{ie}^n\right]_\times \tau_L^v - (\tilde{\omega}_{ib}^b)_\times \tau_L^v + (C_{b'}^b - \mathrm{I}_{3\times3})\tilde{f}_{ib}^b - \\ &\quad \delta f_{ib}^b + (C_n^{b'})^{\mathrm{T}}(2\delta\boldsymbol{\omega}_{ie}^n + \delta\boldsymbol{\omega}_{en}^n)_\times \tilde{\boldsymbol{v}}^n\end{aligned} \tag{26}$$

Due to the different definition of velocity error, the differential equation for the position error in LSE-TCKF is given as follows:

$$\begin{aligned}\frac{\mathrm{d}\delta p_L}{\mathrm{d}t} &= N_{rr}\delta p_L + N_{rv}(\delta v^{\mathrm{n}})\\ &= N_{rr}\delta p_L + N_{rv}(-C_{b'}^n\tau_L^v)\end{aligned} \tag{27}$$

where $N_{rv} = M_1$, N_{rr} is defined as follows:

$$N_{rr} = \begin{bmatrix} 0 & 0 & -\dfrac{\tilde{v}_N}{(R_M+h)^2} \\ \dfrac{\tilde{v}_E\tan L}{(R_N+h)\cos L} & 0 & -\dfrac{\tilde{v}_E}{(R_N+h)^2\cos L} \\ 0 & 0 & 0 \end{bmatrix} \tag{28}$$

Equations (25)–(27) are termed the left-error differential equations of LSE-TCKF, from which the one-step state prediction of LSE-TCKF can be obtained as follows:

$$\bar{x}_k = \sum_{j=1}^{2n}\omega_j f_{\mathrm{LSE}}(\chi_{\mathrm{j}}^+) \tag{29}$$

where $f_{\mathrm{LSE}}(\chi_{\mathrm{j}}^+)$ denotes the state transition equation, which is given as follows:

$$\begin{aligned} f_{\mathrm{LSE}}(\chi_i^+) &= [f(\mathrm{d}\varphi_L)\ f(\mathrm{d}v_L)\ f(\mathrm{d}p_L)\ \mathrm{d}\nabla\ \mathrm{d}\varepsilon]^{\mathrm{T}}\\ &= \begin{bmatrix} \mathrm{d}\varphi_L + [-(\tilde{\omega}_{ib}^b)_\times \mathrm{d}\varphi_L - \mathrm{d}\nabla + C_n^{b'}\delta\omega_{in}^n]T \\ \mathrm{d}v_L + \{-[(C_n^{b'})^{\mathrm{T}}\tilde{\omega}_{ie}^n]_\times \mathrm{d}v_L - (\tilde{\omega}_{ib}^b)_\times \mathrm{d}v_L + (C_{b'}^b - \mathrm{I}_{3\times3})\tilde{f}_{ib}^b \\ -\mathrm{d}\varepsilon + (C_n^{b'})^{\mathrm{T}}(2\delta\omega_{ie}^n + \delta\omega_{en}^n)_\times \tilde{v}^n\}T \\ \mathrm{d}p_L + [N_{rr}\mathrm{d}p_L + N_{rv}(-C_n^{b'}\mathrm{d}v_L)]T \\ \mathrm{d}\nabla \\ \mathrm{d}\varepsilon \end{bmatrix} \end{aligned} \tag{30}$$

Subsequently, the measurement prediction of LSE‑TCKF is derived. According to the definition of left error, the measurement equation of LSE‑TCKF is expressed as follows:

$$z_k = \delta v^n = \tilde{v}^n - v^n = -C_{b'}^n\tau_L^v \tag{31}$$

where z_k denotes the measurement of SINS/DVL, i.e., the velocity difference provided by SINS and DVL. Consequently, the predicted measurement value can be obtained as follows:

$$\bar{z}_k = \sum_{j=1}^{2n}(-C_{b'}^n\chi_{j,v}^-)\omega_j \tag{32}$$

where $\chi_{j,v}^-$ represents the velocity state in χ_j at the j_{th} iteration. According to the definition of left error, the feedback correction of LSE-TCKF can be derived as follows:

$$\begin{cases} C_{b,L}^n = C_{b'}^n\exp(\delta\varphi_L) \\ v_L^n = \tilde{v}^n - \delta v_L^n = \tilde{v}^n + C_{b'}^n\tau_L^v \\ p_L = \tilde{p} - \delta p_L \end{cases} \tag{33}$$

By replacing Equations (3), (12) and (14) in SO(3)-TCKF with Equations (29), (32) and (33), the TCKF based on left-error SE(3), namely LSE-TCKF, can be obtained.

3.3 Right-Error SE(3)-TCKF

This section derives the right-error SE(3)-TCKF (RSE-TCKF). Let the estimated state of the SINS/DVL system by RSE-TCKF with right error be $x_R = [\delta\varphi_R \ \delta v_R \ \delta p_R \ \delta\nabla \ \delta\varepsilon]^{\mathrm{T}}$. Based on Equations (19) and (20), the redefined right-error state satisfying group invariance properties is obtained as follows:

$$\begin{aligned}\tau_R &= \chi\tilde{\chi}^{-1} \\ &= \begin{bmatrix} C_b^n\tilde{C}_n^b & v^n - C_b^n\tilde{C}_n^b\tilde{v}^n \\ 0_{1\times3} & 1 \end{bmatrix} \\ &= \begin{bmatrix} \tau_R^a & \tau_R^v \\ 0_{1\times3} & 1 \end{bmatrix} \in \mathrm{SE(3)}\end{aligned} \tag{34}$$

where τ_R^a and τ_R^v denote the newly defined right-invariant attitude error and velocity error, respectively. Due to different error definitions, similar to LSE-TCKF, RSE-TCKF also differs from SO(3)-TCKF in state prediction, measurement prediction and feedback correction.

First, the state prediction of RSE-TCKF is derived. By differentiating τ_R^a and τ_R^v, the differential equations of attitude and velocity errors for right-error SE(3) are obtained as follows:

$$\begin{aligned}\frac{\mathrm{d}\tau_R^a}{\mathrm{d}t} &= \frac{\mathrm{d}C_b^n\tilde{C}_n^b}{\mathrm{d}t} \\ &= \frac{\mathrm{d}C_{n'}^n}{\mathrm{d}t} \\ &\approx \frac{\mathrm{d}((\delta\varphi_R)_\times)}{\mathrm{d}t} \\ &= -[(\tilde{\omega}_{in}^n)_\times\delta\varphi_R]_\times + (\delta\omega_{in}^n)_\times - (C_b^{n'}\delta\omega_{ib}^b)_\times\end{aligned} \tag{35}$$

$$\frac{\mathrm{d}\delta\varphi_R}{\mathrm{d}t} = -(\tilde{\omega}_{in}^b)_\times\delta\varphi_R + \delta\omega_{in}^n - C_n^{b'}\delta\omega_{ib}^b \tag{36}$$

$$\begin{aligned}\frac{\mathrm{d}\tau_R^v}{\mathrm{d}t} &= \frac{\mathrm{d}(v^n - C_b^nC_{n'}^b\tilde{v}^n)}{\mathrm{d}t} \\ &= -C_{n'}^nC_{n'}^b\delta f_{ib}^b - [(2\delta\tilde{\boldsymbol{\omega}}_{ie}^n + \delta\tilde{\boldsymbol{\omega}}_{en}^n)_\times]\tau_R^v - (C_{n'}^n\tilde{v}^n)_\times(\mathrm{I}_{3\times3} - C_n^{n'})\tilde{\boldsymbol{\omega}}_{ie}^n - \\ &\quad (C_{n'}^n\tilde{v}^n)_\times\delta\tilde{\boldsymbol{\omega}}_{ie}^n + (\mathrm{I}_{3\times3} - C_{n'}^n)\tilde{g}^n - (C_{n'}^n\tilde{v}^n)_\times C_{n'}^b\delta\boldsymbol{\omega}_{ib}^b\end{aligned} \tag{37}$$

where $\tilde{g}^n$ denotes the gravitational acceleration.

Due to the different definition of velocity error, the differential equation of position error in right-error SE(3) is given as:

$$\begin{aligned}\frac{d\delta p_R}{dt} &= N_{rr}\delta p_R + N_{rv}\delta v_R \\ &= N_{rr}\delta p_R + N_{rv}(\tilde{v}^n - C_{n'}^n\tilde{v}^n\tau_R^v)\end{aligned} \tag{38}$$

Based on Equations (36), (37) and (38), the one-step state prediction of RSE-TCKF can be obtained as follows:

$$\bar{x}_k = \sum_{j=1}^{2n}\omega_j f_{\mathrm{RSE}}(\chi_{\mathrm{j}}^+) \tag{39}$$

where $f_{\mathrm{RSE}}(\chi_{\mathrm{j}}^+)$ denotes the state transition equation, which is given as follows:

$$
\begin{aligned}
f_{\mathrm{RSE}}(\chi_i^+) &= [f(\mathrm{d}\varphi_R)\ f(\mathrm{d}v_R)\ f(\mathrm{d}p_R)\ \mathrm{d}\nabla\ \mathrm{d}\varepsilon]^{\mathrm{T}} \\
&= \begin{bmatrix}
\mathrm{d}\varphi_R + [-(\tilde{\omega}_{in}^n)_\times \mathrm{d}\varphi_R + \delta\tilde{\omega}_{in}^n - C_{n'}^b \delta\omega_{ib}^b]T \\
\mathrm{d}v_R + [-C_{n'}^n C_{n'}^b \mathrm{d}\varepsilon - (2\tilde{\omega}_{ie}^n + \tilde{\omega}_{en}^n)_\times \mathrm{d}v_R - (C_{n'}^n \tilde{v}^n)_\times (I_{3\times 3} - C_n^{n'})\tilde{\omega}_{ie}^n - \\
(C_{n'}^n \tilde{v}^n)_\times \delta\tilde{\omega}_{ie}^n + (I_{3\times 3} - C_{n'}^n)\tilde{g}^n - (C_{n'}^n \tilde{v}^n)_\times C_{n'}^b \mathrm{d}\nabla]T \\
\mathrm{d}p_R + [N_{rr}\mathrm{d}p_R - N_{rv}(\tilde{v}^n - C_{n'}^n \tilde{v}^n \mathrm{d}v_R)]T \\
\mathrm{d}\nabla \\
\mathrm{d}\varepsilon
\end{bmatrix}
\end{aligned} \tag{40}
$$

Subsequently, the measurement prediction of RSE‑TCKF is derived. According to the definition of right error, the measurement equation of RSE‑TCKF is expressed as follows:

$$
z_k = \delta v^n = \tilde{v}^n - v^n = \tilde{v}^n - C_{n'}^n \tilde{v}^n - \tau_R^v \tag{41}
$$

Consequently, the predicted measurement value is given as:

$$
\bar{z}_k = \sum_{j=1}^{2n} (\tilde{v}^n - C_{n'}^n \tilde{v}^n - \chi_{j,v}^-)\omega_j \tag{42}
$$

According to the definition of right error, the feedback correction of RSE‑TCKF can be derived as follows:

$$
\begin{cases}
C_{b,R}^n = \exp(\delta\varphi_R) C_b^{n'} \\
v_R^n = \tilde{v}^n - \delta v_R^n = \tilde{v}^n - C_{n'}^n \tilde{v}^{\mathrm{n}} + \tau_R^v \\
p_R = \tilde{p} - \delta p_R
\end{cases} \tag{43}
$$

By replacing Equations (3), (12) and (14) in SO(3)-TCKF with Equations (39), (42) and (43), the TCKF based on right-error SE(3), namely RSE-TCKF, can be obtained.

3.4 Robust Adaptive TCKF Based on SE(3)

By redefining state errors, SE(3)-TCKF alleviates the spatial inconsistency problem of SO(3)-TCKF, yet it remains susceptible to measurement outliers induced by complex external environments, which degrade estimation accuracy. As a widely used robust strategy, the Huber method reconstructs measurement-related information by constructing a nonlinear regression equation and establishing a generalized cost function to suppress the influence of outliers. To further improve the robustness of SE(3)-TCKF and ensure superior state estimation performance, this section constructs different Huber nonlinear regression equations based on the measurement predictions of left-error and right-error SE(3)-TCKF derived in the previous section. The chi-square test and Huber method are adopted to adaptively reconstruct measurements for SE(3)-TCKF, thereby proposing a robust adaptive TCKF based on SE(3) left and right errors, namely SE(3)-RATCKF. In the measurement update stage, SE(3)-RATCKF utilizes the chi-square test to detect measurement innovations in real time. If the test statistic exceeds the chi-square threshold, the measurement is regarded as abnormal, and the Huber method is adaptively activated to reconstruct the outlier measurement; otherwise, no robust processing is performed. Specifically, the robust adaptive improvements of SE(3)-RATCKF are detailed as follows.

(1) After calculating the filtering gain of SE(3)-TCKF, the innovation sequence and chi-square test statistic are constructed from the SINS/DVL measurements as follows:

$$
\begin{cases}
\varepsilon_k = z_k - \bar{z}_k \\
G_k = \varepsilon_k^T (P_k^{zz})^{-1} \varepsilon_k
\end{cases} \tag{44}
$$

where G_k follows a chi-square distribution with d degrees of freedom, where d =3 denotes the measurement dimension. When the measurement information is normal, ε_k is zero-mean Gaussian white noise; otherwise, ε_k deviates with a non-zero mean. The criterion for judging abnormal measurement information is defined as follows:

$$\begin{cases} |G_k| > T_D \Rightarrow \text{Abnormal Measurement Information} \\ |G_k| \le T_D \Rightarrow \text{Normal Measurement Information} \end{cases} \tag{45}$$

where T_D denotes the preset fault threshold, whose value corresponds to a specific false-alarm probability p_f. The correlation between T_D and p_f can be obtained from the chi-square distribution table. A smaller fals-alarm probability p_f indicates higher fault diagnosis capability. In this paper, the false-alarm probability is set to P_f=0.01 for 3 degrees of freedom, which yields the threshold T_D=11.34. When the measurement is abnormal, the Huber estimation is activated, and the Huber tuning constant is set to 1.345, which provides 95% asymptotic efficiency under Gaussian noise. Furthermore, the process noise covariance matrix and the measurement noise covariance matrix are set as Q_k=diag([10^{-8}I$_3$, 10^{-6}I$_3$, 10^{-8}I$_3$, 10^{-8}I$_3$, 10^{-10}I$_3$] and R_k=diag([0.05^2, 0.05^2, 0.05^2]) (in $(\text{m/s})^2$), respectively.

(2) When the measurement information is normal, the state estimation update and covariance update formulas in SO(3)-TCKF are adopted for calculation.

(3) When the measurement information is abnormal, the Huber operation is performed. First, the nonlinear regression equations for left- and right-error SE(3)-RATCKF are constructed. Among them, the nonlinear regression equation of LSE-RATCKF is expressed as follows:

$$\begin{bmatrix} z_k \\ \bar{x}_k \end{bmatrix} = \begin{bmatrix} h_L(x_{v,k}) \\ x_k \end{bmatrix} + \begin{bmatrix} n_k \\ -\delta\bar{x}_k \end{bmatrix} \tag{46}$$

where $\delta\bar{x}_k = x_k - \bar{x}_k$, $h_L(x_{v,k}) = -C_{b'}^{n} x_{v,k}$, and $x_{v,k}$ denotes the velocity state of x_k.

Accordingly, the nonlinear regression equation of RSE-RATCKF is expressed as follows:

$$\begin{bmatrix} z_k \\ \bar{x}_k \end{bmatrix} = \begin{bmatrix} h_R(x_{v,k}) \\ x_k \end{bmatrix} + \begin{bmatrix} n_k \\ -\delta\bar{x}_k \end{bmatrix} \tag{47}$$

where $h_R(x_{v,k}) = \tilde{v}^n - C_{n'}^{n}\tilde{v}^n x_{v,k}$.

Then, the following variables are defined:

$$D_k = \begin{bmatrix} R_k & 0 \\ 0 & P_k^- \end{bmatrix} \tag{48}$$

$$y_k = D_k^{-1/2} \begin{bmatrix} z_k \\ \bar{x}_k \end{bmatrix} \tag{49}$$

$$g(x_k) = D_k^{-1/2} \begin{bmatrix} h(x_{v,k}) \\ x_k \end{bmatrix} \tag{50}$$

$$u_k = D_k^{-1/2} \begin{bmatrix} v_k \\ -\delta\bar{x}_k \end{bmatrix} \tag{51}$$

When the left-error definition is adopted for SINS/DVL, $h(x_{v,k}) = h_L(x_{v,k})$; when the right-error definition is adopted, $h(x_{v,k}) = h_R(x_{v,k})$. The reconstructed measurement information is obtained as follows:

$$\tilde{z}_k = D_k^{1/2}\tilde{y}_k(1:c) = D_k^{1/2}[g(x_k) + \Psi(1:c,1:c)e_k(1:c)] \tag{52}$$

where Ψ denotes the weighting matrix, c is the sum of the dimensions of the state and measurement, $\tilde{y}_k = g(x_k) + \tilde{e}_k$ is the corrected y_k, and $\tilde{e}_k$ is the innovation sequence corrected by the Huber method. Furthermore, the state estimation update under abnormal measurements is performed as follows:

$$\tilde{x}_k = \bar{x}_k + K_k(\tilde{z}_k - \bar{z}_k) \tag{53}$$

Finally, the covariance matrix update under abnormal measurements is performed.

According to the robust adaptive improvement process of SE(3)-RATCKF, the chi-square test activates the Huber method only when measurements are abnormal, avoiding the substitution of $z_k = \tilde{z}_k$ by the Huber method under normal measurement conditions.

4 Experimental Verification of SINS/DVL

To verify the performance of SE(3)-RATCKF, experiments for verifying spatial consistency and the robust adaptive strategy are carried out respectively. During the experiments, a StarNeto XW-IMU5200 (Beijing StarNeto Technology Co., Ltd., China) and a Hi-Target HD-370 DVL (Hi-Target Surveying Instrument Co., Ltd., China) are adopted as experimental devices. Both sensors were factory-calibrated, and a field installation calibration was performed to determine the lever-arm and misalignment angles between the IMU and DVL. Meanwhile, an integrated navigation system composed of a high-precision GPS and IMU is taken as the reference. Ship-borne SINS/DVL integrated navigation tests are conducted on the Yangtze River in Badong County, Hubei Province. The data update frequencies of the IMU and DVL are 200 Hz and 1 Hz respectively, and other key performance parameters are provided by the manufacturers and listed in Table 1. The carrier trajectory and velocity measurements provided by the DVL during navigation are shown in Figure 1 and Figure 2, respectively. As can be seen from Figure 2, velocity measurements obtained by the DVL contain outliers due to complex environmental factors such as water-surface fluctuations.

Table 1 Parameters of SINS/DVL integrated navigation shipboard test sensor

sensor	error term	error value
IMU	accelerometer drift (ug)	≤50
IMU	gyro drift (°/h)	≤0.02
DVL	position error (m)	≤10
DVL	velocity error (m/s)	≤0.005(approx. ≤ 0.1% of measurement)

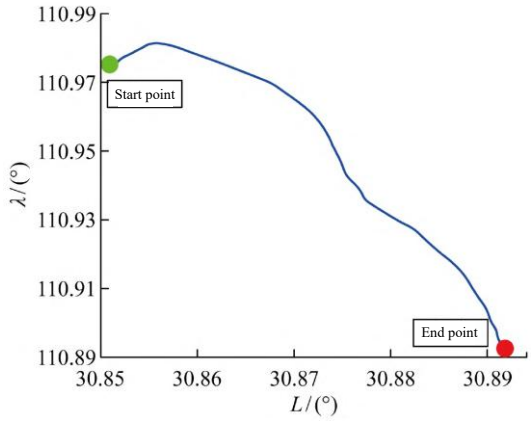


Figure 1 Carrier trajectory

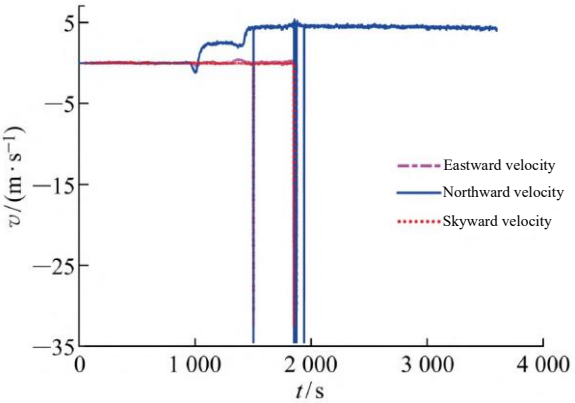


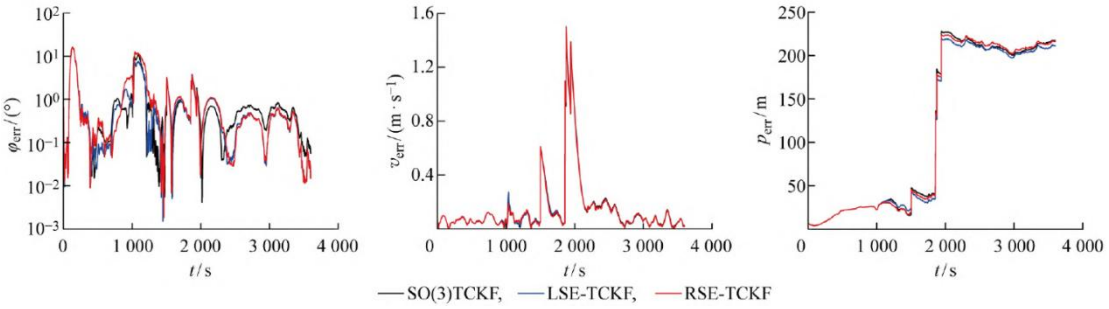
Figure 2 Measurement information

4.1 Spatial Consistency Experiment of SE(3)-TCKF

It should be noted that the ship-borne field test data used in this section inherently contains real DVL outliers caused by complex environmental disturbances (as shown in Fig. 2). Therefore, the spatial consistency experiments under large misalignment angles are conducted in a realistic environment with actual measurement anomalies. The increase in misalignment angles exacerbates the inconsistency between the ideal coordinate system and the computational coordinate system. In this section, the state estimation performance of SO(3)-TCKF, LSE-TCKF and RSE-TCKF under different misalignment angles is compared to verify the state-space consistency of SE(3)-TCKF. The initial misalignment angles are set to (0°, 0°, 0°), (5°, 5°, 10°), (25°, 25°, 25°) and (30°, 30°, 45°), respectively. The attitude, velocity and position errors are calculated as follows:

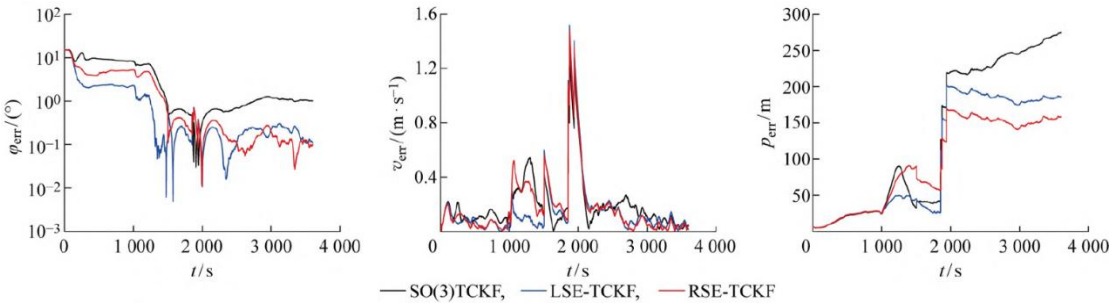
$$\begin{cases} \varphi_{err} = \sqrt{(\theta_{err})^2 + (\gamma_{err})^2 + (\psi_{err})^2} \\ v_{err} = \sqrt{(v_{err}^E)^2 + (v_{err}^N)^2 + (v_{err}^U)^2} \\ p_{err} = \sqrt{(L_{err})^2 + (\lambda_{err})^2} \end{cases} \tag{54}$$

where θ_{err}, γ_{err}, and ψ_{err} denote the pitch angle error, roll angle error, and yaw angle error, respectively; v_{err}^E, v_{err}^N, and v_{err}^U represent the velocity errors in the east-north-up (ENU) frame; L_{err} and λ_{err} are the latitude error and longitude error, respectively. The navigation errors of the three methods are illustrated in Figs. 3–6, with the corresponding root-mean-square errors (RMSEs) listed in Tables 2–5. The accuracy improvement ratios of LSE-TCKF and RSE-TCKF relative to SO(3)-TCKF under varying misalignment angles are given in Table 6.



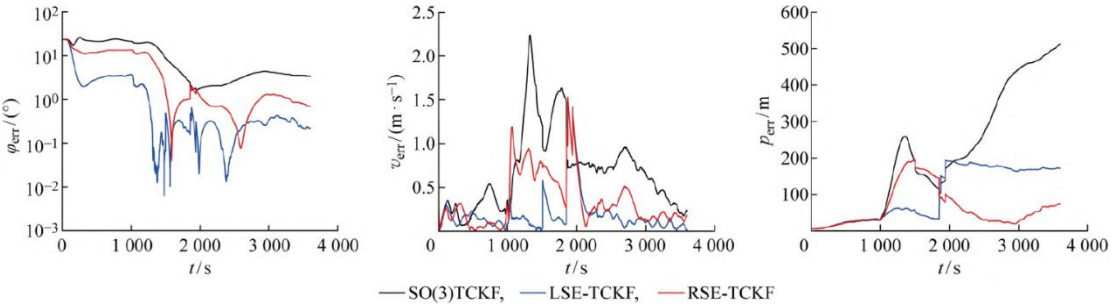
(a) attitude error (b) velocity error (c) position error

Figure 3 Navigation error at a misalignment angle of (0°, 0°, 0°) (Attitude error axis in log scale.)



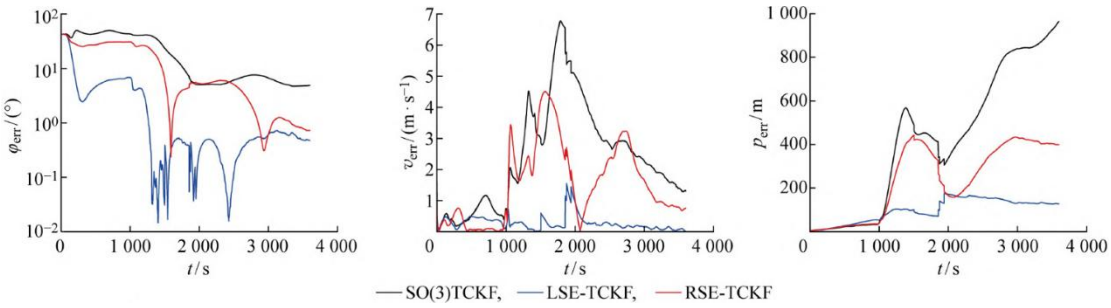
(a) attitude error (b) velocity error (c) position error

Figure 4 Navigation error at a misalignment angle of (5°, 5°, 10°) (Attitude error axis in log scale.)



(a) attitude error (b) velocity error (c) position error

Figure 5 Navigation error at a misalignment angle of (25°, 25°, 25°) (Attitude error axis in log scale.)



(a) attitude error (b) velocity error (c) position error

Figure 6 Navigation error at a misalignment angle of (30°, 30°, 45°) (Attitude error axis in log scale.)

Table 2 RMSE at a misalignment angle of (0°,0°,0°)

type	attitude error (°)	velocity error (m/s)	position error (m)
SO(3) TCKF	0.4398	0.2701	148.1477
LSE-TCKF	0.4063	0.2726	145.2220
RSE-TCKF	0.4898	0.2705	148.5562

Table 3 RMSE at a misalignment angle of (5°, 5°, 10°)

type	attitude error (°)	velocity error (m/s)	position error (m)
SO(3) TCKF	5.7216	0.2823	168.3880
LSE-TCKF	2.8864	0.2800	130.7681
RSE-TCKF	3.7629	0.2916	112.6266

Table 4 RMSE at a misalignment angle of (25°, 25°, 25°)

type	attitude error (°)	velocity error (m/s)	position error (m)
SO(3) TCKF	13.7960	0.8252	267.4668
LSE-TCKF	4.4413	0.2948	124.6077
RSE-TCKF	8.3495	0.4619	83.1753

Table 5 RMSE at a misalignment angle of (30°,30°,45°)

type	attitude error (°)	velocity error (m/s)	position error (m)
SO(3) TCKF	28.5392	2.9457	530.9850
LSE-TCKF	8.2675	0.3681	111.9661
RSE-TCKF	18.5396	1.9763	291.0149

Table 6 Percentage improvement in accuracy of LSE-TCKF and RSE-TCKF compared to SO(3) TCKF at variations in misalignment angle

misalignment angle	algorithm	attitude accuracy improvement ratio (%)	velocity accuracy improvement ratio (%)	position accuracy improvement ratio (%)
(5°, 5°, 10°)	LSE-TCKF	49.55	-3.29	22.34
(5°, 5°, 10°)	RSE-TCKF	34.23	0.81	33.11

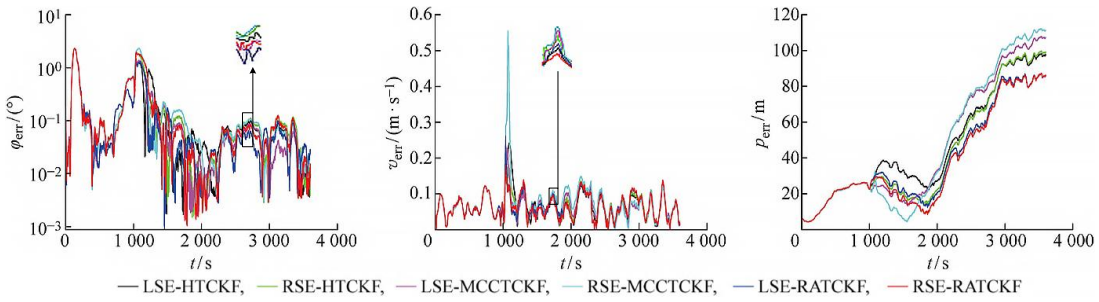
(25°, 25°, 25°)	LSE-TCKF	67.81	64.28	53.41
(25°, 25°, 25°)	RSE-TCKF	39.48	44.03	68.91
(30°, 30°, 45°)	LSE-TCKF	71.03	87.51	78.91
(30°, 30°, 45°)	RSE-TCKF	35.04	32.91	45.19

It can be seen from Figure 3 and Table 2 that when the misalignment angles are (0°, 0°, 0°), the differences in attitude, velocity and position errors among SO(3)-TCKF, LSE-TCKF and RSE-TCKF are minor. This is because the directional inconsistency of the coordinate system in SO(3)-TCKF is negligible under small misalignment angles. As shown in Figures 4–6 and Tables 3–5, the directional discrepancy between the ideal coordinate system and the computational coordinate system becomes increasingly prominent with the gradual increase of misalignment angles, which degrades the estimation performance of SO(3)-TCKF. In contrast, LSE-TCKF and RSE-TCKF incorporate system states into a unified coordinate system, both mitigating the spatial inconsistency of SO(3)-TCKF. Table 6 indicates that the performance advantages of LSE-TCKF and RSE-TCKF become more significant as misalignment angles rise, with LSE-TCKF exhibiting relatively superior performance. The improvement of RSE-TCKF increases at misalignment angles of (5°, 5°, 10°) and (25°, 25°, 25°), yet declines at (30°, 30°, 45°). This is attributed to the fact that velocity measurements provided by DVL are weak observations, which are susceptible to disturbances from other information, such as gyroscope and accelerometer biases, wind, waves, and ocean currents. Therefore, the "invariant observation" theory is not applicable to SINS/DVL integrated navigation under certain circumstances. Based on the estimation results of navigation parameters under various misalignment angles, it is verified that SE(3)-TCKF effectively resolves the spatial inconsistency problem of SO(3)-TCKF.

It is worth noting that although the position error itself remains a Euclidean state in the proposed framework, the position estimation accuracy is still significantly improved, as shown in Figs. 3-6. This is because the position is obtained by integrating the velocity over time. By embedding the velocity error into the SE(3) manifold, the spatial consistency of the velocity state directly prevents the accumulation of position errors, thereby effectively improving the integrated position accuracy without needing to adopt the more complex $SE_2(3)$ formulation that explicitly embeds the position state.

4.2 Verification Experiment of Robust Adaptive Strategy

To verify the effectiveness of the robust adaptive improvement, the misalignment angles are fixed at (0°, 0°, 0°) to ensure that the navigation performance is only affected by abnormal measurements (outliers). SE(3)-TCKF, SE(3)-HTCKF (SE(3)-TCKF based on the Huber method), SE(3)-MCCTCKF (SE(3)-TCKF based on the maximum correntropy criterion), and SE(3)-RATCKF are separately adopted to estimate the attitude, velocity and position of the carrier. Herein, SE(3)-HTCKF is a general term for LSE-HTCKF and RSE-HTCKF, while SE(3)-MCCTCKF collectively refers to LSE-MCCTCKF and RSE-MCCTCKF. The navigation errors of different improved strategies are shown in Figure 7, and the corresponding RMSE values are listed in Table 7.



(a) attitude error (b) velocity error (c) position error

Figure 7 Comparison of navigation errors of different improvement strategies (Attitude error axis in log scale.)

Table 7 RMSE of different improvement strategies

type	attitude error (°)	velocity error (m/s)	position error (m)
LSE-HTCKF	0.3959	0.0776	54.7163
RSE-HTCKF	0.4544	0.0741	53.2661
LSE-MCCTCKF	0.4010	0.0733	58.2928
RSE-MCCTCKF	0.5193	0.0918	59.9575
LSE-RATCKF	0.3885	0.0713	48.0363
RSE-RATCKF	0.4748	0.0711	46.7557

It can be observed from Figures 3, 7 and Tables 2, 7 that SO(3)-TCKF and SE(3)-TCKF are susceptible to measurement outliers and exhibit relatively large estimation errors since no robust strategies are introduced. By incorporating the Huber method or maximum correntropy criterion, SE(3)-HTCKF, SE(3)-MCCTCKF and SE(3)-RATCKF possess strong robustness. Comparing the estimation errors of each method in Figure 7 and Table 7, it can be found that SE(3)-RATCKF adaptively activates the Huber estimation only when measurement information is abnormal via chi-square test. This avoids excessive compensation caused by continuous reconstruction in SE(3)-HTCKF under normal measurement conditions, yielding the optimal improvement for LSE-TCKF and RSE-TCKF, followed by the Huber method, with the maximum correntropy criterion performing the worst. Consequently, the proposed robust adaptive strategy can effectively address the problem of measurement outliers in SINS/DVL integrated navigation, further improving the estimation accuracy and robustness of SE(3)-TCKF.

Furthermore, it is worth discussing the combined effect of the SE(3) formulation and the robust adaptive strategy. The SE(3) error state definition fundamentally addresses the spatial inconsistency in the prediction and update steps under large misalignment angles, while the chi-square test and Huber method act specifically on the measurement update stage to suppress outliers. These two mechanisms operate in a decoupled and complementary manner. When large misalignment angles and outliers occur simultaneously, the SE(3) formulation ensures the consistency of state propagation, and the robust mechanism ensures the reliability of the measurement correction. The real-world field data in Section 4.1 (which inherently contains environmental outliers) and the controlled outlier experiments in Section 4.2 collectively demonstrate the effectiveness of this combined architecture.

5 Conclusion

Based on the Lie group theory, this paper integrates state variables such as attitude errors and velocity errors estimated by SO(3)-TCKF into a unified coordinate system, derives the left-right error states, measurement update equations and feedback correction in the SE(3) space, and proposes the SE(3)-based TCKF, which improves the state-space consistency of SO(3)-TCKF. Aiming at the problem that abnormal measurements are easily introduced in SINS/DVL integrated navigation, the chi-square test and Huber method are incorporated into SE(3)-TCKF.

By detecting the measurement innovations of SE(3)-TCKF via chi-square test, the Huber estimation is adaptively activated or deactivated to enhance the robustness of SE(3)-TCKF, thereby developing SE(3)-RATCKF, namely the SE(3)-TCKF with a robust adaptive strategy. Experimental results of SINS/DVL integrated navigation demonstrate that the proposed method can effectively address the issues of state-space inconsistency and measurement anomalies in SO(3)-TCKF, avoid excessive reconstruction of the conventional Huber method under normal measurement conditions, and achieve high robustness and estimation accuracy. Future research will focus on further investigating the practicality of the proposed algorithm. It should be noted that the quantitative results in this study are derived from a single ship-borne field test. Due to the irreproducibility of physical environments, future work will involve Monte Carlo simulations to further validate the statistical properties and confidence intervals of the proposed algorithm.

Data availability

The datasets used and/or analysed during the current study available from the corresponding author on reasonable request.

Funding declaration

No funding was received for this study.

Reference

[1] GAO H L, YOU J, CAO S Y. In-flight alignment method of integrated SINS/GPS navigation system based on combined PF-UKF filter[J]. Journal of Shanghai Jiao Tong University, 2022, 56(11): 1447-1452.

[2] ZHU J, LI A, QIN F, et al. A new robust adaptive filter aided by machine learning method for SINS/DVL integrated navigation system[J]. Sensors, 2022,\\22(10):3792-3813.

[3] YARLY X, XU X, YANG D, et al. An IMM-UKF aided SINS/USBL calibration solution for underwater vehicles[J]. IEEE Transactions on Vehicular Technology, 2020, 69(4): 3740-3747.

[4] NORDIN M H, SHARMA S, KHAN A, et al. Collaborative unmanned vehicles for inspection, maintenance, and repairs of offshore wind turbines[J]. Drones, 2022, 6(6): 137-163.

[5] GAN W, ZHU J, JI D. QPSO-model predictive control-based approach to dynamic trajectory tracking control for unmanned underwater vehicles[J]. Ocean Engineering, 2018, 158: 208-220.

[6] ZHANG W J, MA X. A sliding window adaptive filtering algorithm for autonomous navigation of the approach phase of deep space probe[J]. Journal of Shanghai Jiao Tong University, 2022, 56(11): 1461-1469.

[7] JIANG J H, CHEN G. Dynamic model predictive control method for steering control of driving robot[J]. Journal of Shanghai Jiao Tong University, 2022, 56(5): 594-603.

[8] ZHAO W, ZHAO H, LIU G, et al. ANFIS-EKF based single-beacon localization algorithm for AUV[J]. Remote Sensing, 2022, 14(20): 5281-5301.

[9] ALB N, GAVRILOV A. A novel approach for aiding unscented Kalman filter for bridging GNSS outages in integrated navigation systems[J]. Navigation, 2021, 68(3): 521-539.

[10] YANG J, GAO S, LI G, et al. An adaptive cubature Kalman filtering algorithm based on variational mode decomposition for pulsar navigation[J]. IET Communications, 2022, 16(16): 1982‐1992.

[11] QIN K, DONG X M, CHEN Y, et al. Modified CKF algorithm based on orthogonal transformation[J]. Control and Decision, 2018, 33(2): 330-336.

[12] ZHAO L, XUE J P. Improved CKF based on orthogonal transformation[J]. Computer Engineering and Applications, 2018, 54(18): 45-51.

[13] YAN G M, YAN W S, XU D M. A SINS nonlinear error model reflecting better characteristics of SINS errors[J]. Journal of Northwestern Polytechnical University, 2009, 27(4): 511-516.

[14] WANG M S, WU W Q, HE X F, et al. Further explanation and application of state transformation extended Kalman filter[J]. Journal of Chinese Inertial Technology, 2019, 27(4): 499-504.

[15] ISERLES A, MUNTHE-KAAS H Z, NORSETT S P, et al. Lie-group methods[J]. Acta Numerica, 2000, 9: 215-365.

[16] CUI J, WANG M, WU W, et al. Lie group based nonlinear state errors for MEMS-IMU/GNSS/magnetometer integrated navigation[J]. Journal of Navigation, 2021, 74(4): 887-900.

[17] CHANG L, DI J, QIN F. Inertial based integration with transformed INS mechanization in earth frame[J]. IEEE/ASME Transactions on Mechatronics, 2021, 27: 1738-1749.

[18] QIAN L, QIN F, LI K, et al. Research on the necessity of lie group strapdown inertial integrated navigation error model based on Euler angle[J]. Sensors, 2022, 22(20): 7742-7761.

[19] AXEL B, SILVERE B. Invariant Kalman filtering[J]. Annual Review of Control, Robotics, and Autonomous Systems, 2018, 1(1): 237-257.

[20] LUO Y, GUO C, LIU J. Equivariant filtering framework for inertial-integrated navigation[J]. Satellite Navigation, 2021, 2: 1-17.

[21] WANG M, WU W, ZHOU P, et al. State transformation extended Kalman filter GPS/SINS tightly coupled integration[J]. GPS Solutions, 2018, 22: 1-12.

[22] DU S, HUANG Y, LIN B, et al. A lie group manifold-based nonlinear estimation algorithm and its application to low-accuracy SINS/GNSS integrated navigation[J]. IEEE Transactions on Instrumentation and Measurement, 2022, 71: 1-27.

[23] ZHU T, LI A, LI K, et al. The quaternion based error model based on SE(3) of the INS[J]. IEEE Sensors Journal, 2022, 22(13): 13067-13077.

[24] FAN X, WANG G, HAN J, et al. Interacting multiple model based on maximum correntropy Kalman filter[J]. IEEE Transactions on Circuits and Systems II—Express Briefs, 2021, 68(8): 3017-3021.

[25] ZHU B, CHANG L, XU J, et al. Huber-based adaptive unscented Kalman filter with non-Gaussian measurement noise[J]. Circuits, Systems, and Signal Processing, 2018, 37(9): 3842-3861.

[26] ZHANG W J, WANG S Y, FENG Y L, et al. Huber-based high-degree cubature Kalman tracking algorithm[J]. Acta Physica Sinica, 2016, 65(8): 358-366.

[27] HUANG Y, WU L H, SUN F. Robust Cubature Kalman filter based on Huber M-estimator[J].

Control and Decision, 2014, 29(3): 572-576.

[28] LIU M M, LIU J L, XIN S W. Robust Adaptive Autonomous Navigation Method Under Multi-Path Delay Calculation[J]. Journal of Marine Science and Engineering, 2026, 14(7): 654.